ESAPS Materials:

Supporting Online Materials include 1) Time-evolution of transonic and supersonic fuel jets and shock waves generated by them quantitatively visualized by microsecond x-radiography in avi format; 2) Description of reconstruction of gas mass distribution in Mach cone; 3) Methods of multiphase computational fluid dynamics simulation; 4) Multiphase computational fluid dynamics simulation results of shock waves generated by liquid fuel jets injected at 40, 100, and 135 MPa in a form of animation; and 5) Calculation of conservation of excess gas mass near the shock-wave front.

Supplementary Material #1: Time-evolution of transonic and supersonic fuel jets and shock waves generated by them quantitatively visualized by microsecond x-radiography.

SM #1.avi.

Supplementary Material #2: Reconstruction of gas mass distribution in Mach cone

The x-radiographs of the shock wave line-of-sight projection are quantitative; one can use single-projection reconstruction methods to calculate the gas distribution near and inside the cone based on an axial symmetric mode illustrated in Figure SM1. For monochromatic x-rays transmitting through a nonuniformly distributed material, the analysis of the transmission of the attenuating material is straightforward, given by $I/I_0 = \exp(-\mu_M M)$, where I and I_0 are the transmitted and incident x-ray intensities, respectively; μ_M is the mass absorption coefficient, which can be measured and calibrated accurately for the absorbing medium (ambient gas) at the single wavelength; and M is the mass of fuel in the beam. Thus, the time evolution of the measured x-ray transmission I/I_0 can be simply transformed into integrated, line-of-sight fuel mass data at each point in the radiograph. The Mach cone is illustrated in Figure SM1a, where the cone angle is α, depending on the jet leading-edge speed. The calculated gas density distribution can be used to compare with the results from the CFD simulation. Due to the low signal-to-noise ratio of the absorption data, it is only possible to use a model-dependent reconstruction rather than the conventional single-view tomographic reconstruction techniques. The following assumptions are used in the reconstruction: 1) the gas distribution is axisymmetrical; 2) the cross-sectional distribution of the compressed gas is composed of two Gaussian distributions (inner and outer sides) with two respective widths; 3) inside the Mach

cone (behind the shockwave front) the excess gas density is negative, indicating a decompression region near the cone axis; and 4) the peak gas density at each cross section decreases linearly with the distance to the cone tip. Referring to Figure SM1, therefore, the gas density $\rho(r,z,t)$ near the cone, in polar coordinates, is described by

$$\rho(r,z,t)=\left[\rho_0(z,t)+\rho_-(z,t)\right]e^{-\frac{\left[r-r_-(z,t)\right]^2}{\sigma_1^2(t)}}-\rho_-(z,t), \quad \text{if } r\le r_0(z,t)$$
$$\rho(r,z,t)=\rho_0(z,t)e^{-\frac{\left[r-r_-(z,t)\right]^2}{\sigma_2^2(t)}}, \quad \text{if } r>r_0(z,t),$$

where $\rho_0(z,t)$ is the peak density at the cross section at an axial distance at *z* with $\rho_0(z,t)\propto\frac{1}{z}$, $\rho_-(z,t)$ is the decompression offset inside the Mach cone near the axis, and σ_1 and σ_2 are the Gaussian width on the inner and outer sides of the cone, respectively. Since the x-radiography images were produced with parallel x-ray beam along the x-direction in Cartesian coordinates, the projected 2-dimensional gas mass distribution $M(y,z,t)$ in the y-z plane can be obtained by integrating the density along the x-direction, $M(y,z,t)=A\int\rho(r,z,t)dx$, where A is a constant related to the pixel size of the detector.

The so-calculated $M(y,z,t)$ was fit to experiment radiography data to yield the fitting parameters $\rho_0(z,t)$, $\rho_-(z,t)$, σ_1, and σ_2, which describe the reconstructed gas distribution. We note that it is ***absolutely*** necessary to include $\rho_-(z,t)$ in the model. Otherwise, it would be impossible to fit the radiographic data on the inner side of the Mach cone.

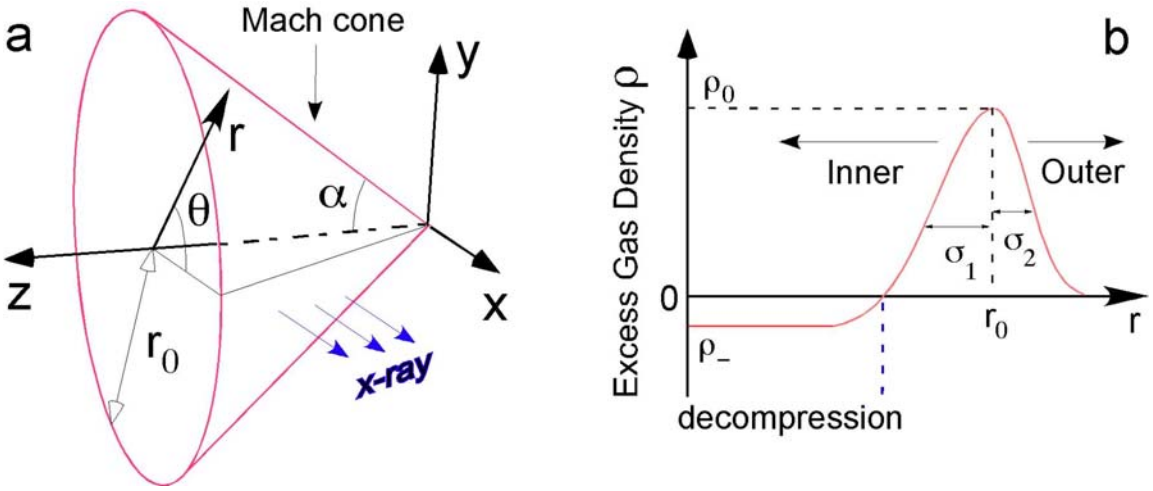

Figure SM1. Model-dependent reconstruction of the gas density near the Mach cone: a) coordinate systems associated with the model, b) gas density model at a cross section perpendicular to the cone axis.

Supplementary Material #3: Multiphase computational fluid dynamics simulation

Gas phase equations

The governing equations for the gas phase in the numerical simulation are the two-dimensional Euler equations in axial symmetric geometry. The vector form of the equations is given by

$$\frac{\partial \vec{u}}{\partial t}+\frac{\partial F(\vec{u})}{\partial x}+\frac{\partial G(\vec{u})}{\partial y}=H(\vec{u})+S(\vec{u}), \qquad (1)$$

where x and $y\geq 0$ are the axial and radial coordinates, respectively; and t is the evolution time of the jet. The flow variable vector $\vec{u}$, the flux vectors $F(\vec{u})$ and $G(\vec{u})$, the source term $H(\vec{u})$ due to axial symmetric geometry, and $S(\vec{u})$ the exchange term between the gas and moving particles, can be described as:

$$\vec{u} = \left[\rho, \rho u, \rho v, \rho E\right]^T, \qquad (2a)$$

$$F(\vec{u}) = \left[\rho u, \rho u^2+p, \rho uv, (\rho E+p)u\right]^T, \qquad (2b)$$

$$G(\vec{u}) = \left[\rho v, \rho uv, \rho v^2+p, (\rho E+p)v\right]^T, \qquad (2c)$$

$$H(\vec{u}) = -\frac{1}{y}\left[\rho v, \rho uv, \rho v^2, (\rho E + p)v\right]^T, \tag{2d}$$

$$S(\vec{u}) = \left[0, M_x, M_y, Q_e\right]^T, \tag{2e}$$

where ρ, u, v, p, and E represent density, axial velocity, radial velocity, pressure, and total specific energy for gas phase, respectively. The total specific energy E is defined as

$$E = e + \frac{1}{2}\left(u^2 + v^2\right), \tag{3}$$

where $e = p/(\gamma - 1)$ is the internal energy of the gas phase, and $\gamma = c_p / c_v$ is the capacity ratio between specific heats.

The exchange coupling terms on the right-hand side of the governing equation account for the particle interaction effects for each individual conservative equation. In the continuity equation, which is the first component in Eq. (1), there is no source term since we assume non-evaporating spray. M_x and M_y in the momentum equations are the terms defining the momentum exchanges in the x and y directions between the spray and gas per unit volume. In addition, the term Q_e in the energy equation represents the energy exchange between the droplets and the gas phase accounting for total energy, heat transfer, and heat of vaporization. Here, kinetic energy due to the supersonic speed of the spray was considered. As a result, the source terms in the momentum and energy equation can be summarized by taking ensemble averages in each control volume if an individual particle is labeled by subscript *k*:

$$M_i = -\sum_k D_k(\vec{u})(\vec{u} - \vec{u}_k)\delta(\vec{x} - \vec{x}_k), \quad i = x, y, \tag{4}$$

$$Q_e = -\sum_k D_k(\vec{u})\left[(\vec{u} - \vec{u}_k)\cdot\vec{u}_k\right]\delta(\vec{x} - \vec{x}_k), \tag{5}$$

where the summations represent the total number of particles in the calculation cell, δ(x) is the Dirac delta function, and $D_k(\vec{u})$ is the drag function, which will be described in the spray equation.

Dispersed phase equations

In a Lagrangian reference frame, each computational particle, individually labeled by subscript *k*, represents a number of droplets with the same size, position, and velocity. This is

required in the discrete particle method described in detail in [20]. As a result, the required equation to trace the position for each individual droplet is given by

$$\frac{d\vec{x}_k}{dt} = \vec{u}_k \,. \tag{6}$$

Next, the droplet velocity at an arbitrary time instant is determined by solving its momentum equation as

$$m_k \frac{d\vec{u}_k}{dt} = m_k \vec{g} + D_k\left(\vec{u}\right)\left(\vec{u} - \vec{u}_k\right). \tag{7}$$

Here, $m_k (= \frac{4}{3}\pi\rho r_k^3$, where r is droplet radius) is the droplet mass, $\vec{g}\left(\approx 9.8\ m/s^2\right)$ is the standard gravity for droplets, and we assume no turbulent effects on the droplet trajectory, i.e., no turbulent dispersion. In addition, $D_k\left(\vec{u}\right)$ is the drag function

$$D_k\left(\vec{u}\right) = \frac{1}{2}\pi r_k^2 \rho_g C_D \left|\vec{u} - \vec{u}_k\right|. \tag{8}$$

In Eq. (8), the drag coefficient C_D is determined as

$$\begin{aligned} C_D &= \frac{24}{\mathrm{Re}_k}\left[1.0 + 0.15\,\mathrm{Re}_k^{0.687}\right], \qquad \mathrm{Re}_k < 10^3 \\ &= 0.44 \qquad\qquad\qquad , \qquad \mathrm{Re}_k > 10^3 \end{aligned} \tag{9}$$

where Re_k is the particle Reynolds number, which is evaluated by using the relative velocity between the gas and the droplet, i.e.,

$$\mathrm{Re_k} = \frac{2r_k \left|\vec{u} - \vec{u}_k\right| \rho_g}{\mu}. \tag{10}$$

Note that in the present study, Eqs. (6) through (10) are used to simulate the shock-wave generation in conjunction with the gas phase equations.

Numerical scheme

The space-time Conservation Element Solution Element (CESE) method [19] has been applied to solve the spray-shock interaction flow. The space-time CESE method is a high-resolution and genuinely multidimensional method for solving conservation laws. It has a solid foundation in physics such as local and global flux conservation in space and time and yet is mathematically simple. Its nontraditional features are: (i) a unified treatment of space and time,

(ii) the introduction of a conservation element (CE) and a solution element (SE) as the vehicles for enforcing space-time flux conservation, and (iii) a time marching strategy that has a space-time staggered stencil at its core and, as such, can capture shocks without using Riemann solvers. Note that conservation elements are non-overlapping space-time subdomains introduced such that (i) the computational domain can be filled by these subdomains, and (ii) flux conservation can be enforced over each of them and also over the union of any combination of them. On the other hand, solution elements are non-overlapping space-time subdomains introduced such that (i) the boundary of any CE is covered by a combination of SEs, and (ii) within an SE, any physical flux vector is approximated using a simple smooth function.

Supplementary Material #4: Multiphase computational fluid dynamics simulation results of shock waves generated by liquid fuel jets injected at 40, 100, and 135 MPa in a form of animation.

SM #4.avi.

Supplementary Material #5: Conservation of excess gas mass near the shock-wave front.

To further examine the conservation, we randomly selected several snapshots in time from the numerical simulation. Referring to Figure SM2, the interaction of the excess gas density for compression (+ sign) and decompression (- sign) areas was conducted from the shock front to the nozzle exit (x = 0 mm) in three-dimensional space. The range in the radial direction was chosen from 1 to 5 mm from the jet axis where most of the excess gas mass was accounted for.

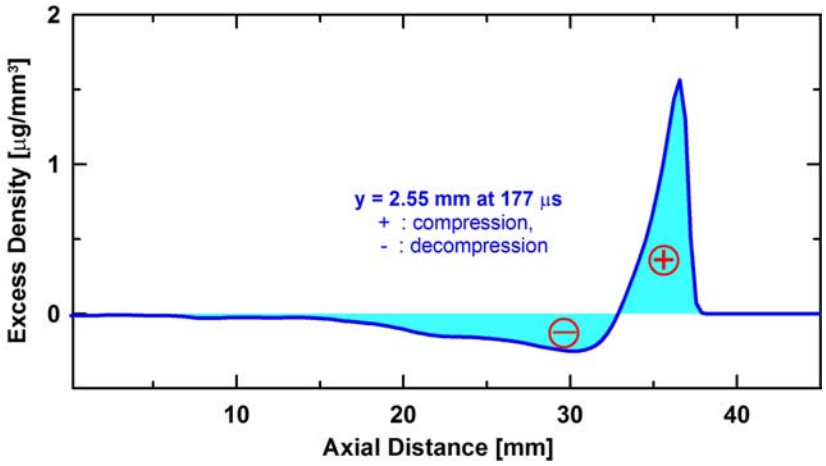

Figure SM2. Integration schematics of the excess density for the compression and decompression areas generated by shockwave at y = 2.55 mm from the spray axis at time 177 μs after SOI and injection pressure of 100 MPa.

Table 1 shows the results at 146, 161, 177, and 183 μs after SOI. The conservation between compression and decompression is demonstrated with very slight residuals.

Table 1. Gas density integrated in three dimensions at an injection pressure of 100 MPa

Time after SOI	Compression density $\times 10^{-7}$ kg/m^3	Decompression density $\times 10^{-7}$ kg/m^3	Residual %
146 μs	1.25	-1.31	-5.98
161 μs	1.54	-1.62	-7.79
177 μs	1.88	-1.97	-9.74
183 μs	2.06	-2.16	-1.07